# Characterisation of Cancer Onset and Development in the TRAMP Model of Prostate Cancer using Diffusion-Weighted Magnetic Resonance Imaging

| | |
|---|---|
| Journal: | *Journal of Magnetic Resonance Imaging* |
| Manuscript ID: | Draft |
| Wiley - Manuscript type: | Original Research |
| Classification: | Diffusion and perfusion imaging < Imaging Principles and Education < Basic Science, Imaging techniques and processing < Imaging technology and safety < Basic Science, Cancer < Body imaging < Clinical Science, Correlative imaging < New Developments < Clinical Science |
| Manuscript Keywords: | prostate cancer, diffusion weighted MRI, transgenic adenocarcinoma of the mouse prostate, cancer screening, ADC, TRAMP |
| | |



# Characterisation of Cancer Onset and Development in the TRAMP Model of Prostate Cancer using Diffusion-Weighted Magnetic Resonance Imaging

## Abstract

**Purpose:** There is a need to improve prostate cancer diagnosis tools to aid clinical decision-making. Diffusion-weighted Magnetic Resonance Imaging (DW-MRI) is sensitive to water diffusion throughout tissues, and has been shown to correlate with Gleason score, a histological measure of prostate cancer aggressiveness. **In this study**, the ability of DW-MRI to detect prostate cancer onset, and disease monitoring was evaluated in TRAMP mice.

**Materials and Methods:** Anatomical and DW-MRI were performed on TRAMP and C57BL/6 control mice from 8 weeks of age until termination at 28-30 weeks. Upon termination, the genitourinary tract was excised, and registered histology slides allowed for validation of DW-MRI to act as a marker of cancer onset.

**Results:** DW-MRI differentiated between normal prostate, well-differentiated, and poorly differentiated cancer. An automated screening tool was developed, which clearly identified early-onset of suspicious prostate regions and visualised their progression to cancer.

**Conclusion:** DW-MRI is a robust tool for detecting the onset of cancer, and discriminating between cancer stages in the TRAMP model. The incorporation of DW-MRI-based prostate cancer stratification and monitoring will increase the accuracy of preclinical trials using TRAMP mice. The study also suggests a role for DW-MRI in monitoring disease progression in patients with low-risk prostate cancer.


**Keywords:** prostate cancer, diffusion weighted MRI, transgenic adenocarcinoma of the mouse prostate, cancer screening, ADC, TRAMP

## Introduction

Prostate cancer (PCa) is the most common malignancy among men in the USA and Europe, and constitutes a substantial healthcare problem (1). Recent advances in PCa diagnosis, including PSA screening and multiparametric magnetic resonance imaging (MRI), have increased our ability to detect the disease at an early stage (2). While this expansion of the therapeutic window increases the number of treatment options for patients, it also emphasises the need for diagnostic tools, including biomarkers, which can aid clinical decision-making based on risk assessment and longitudinal disease monitoring. The continued improvement of PCa diagnosis and treatment relies on developing our understanding of the disease, and of robust experimental systems for the evaluation of new diagnostic tools and treatments.

The transgenic adenocarcinoma of the mouse prostate (TRAMP) model is a genetically engineered model of PCa and a robust platform to evaluate novel chemopreventive and anti-tumour strategies. This model morphologically recapitulates the progression of the human disease (3-6), exhibiting prostatic intraepithelial neoplasia (PIN) between 6-12 weeks old, which develops into well-differentiated adenocarcinomas by 18 weeks, and into poorly differentiated adenocarcinoma with metastasis to the iliac lymph nodes and lungs by 24 to 30 weeks (3-7).

While palpation or terminal genitourinary weight can be used in a high throughput manner to evaluate the efficacy of novel therapeutics in large established tumours in TRAMP mice, they are particularly insensitive to detection of early-stage disease and inadequate for accurate quantitation. Without suitable tools for longitudinal screening, the design of robust preclinical trials evaluating chemoprevention, or novel drugs targeting early stage disease, will be challenging due to variation in cancer onset times and development rates. As a result, there is an

increasing need to establish and evaluate novel non-invasive methods that describe onset and progression of PCa in TRAMP mice in more detail.

MRI is a non-invasive imaging technique, used in both pre-clinical and clinical exams to diagnose and stage PCa (8-11). However, small lesions are difficult to detect, and it is not possible to follow progression from PIN to well-differentiated disease with anatomical imaging alone. Diffusion-weighted (DW) -MRI and the derived biomarker, the apparent diffusion coefficient (ADC), are sensitive to the ease of water diffusion throughout tissues. ADC has been shown to correlate with Gleason score, a histological measure of PCa aggressiveness, and helps to identify patients at risk of developing PCa (12).

The ability to stratify individual tumours is of increasing importance, where the heterogeneous nature of cancer is influenced by both genetic and environmental factors (13-15). In light of the importance of understanding not only this cancer but also its evolution, it is critical to be able to non-invasively characterise tumour heterogeneity and to monitor the progression of disease from pre-cancerous lesions into later stages.

**In this study,** we evaluated the ability of DW-MRI to detect the presence and location of early onset of PCa, and to monitor disease progression in TRAMP mice.

## Materials and Methods

**Ethics:** All experimental procedures involving animals were approved by the Norwegian authority on animal welfare (Application ID 6681) and were in accordance with Norwegian and EU guidelines for the care and use of laboratory animals.

**Animals:** TRAMP (n = 10) and control (n = 6) mice from the same genetic background (C57BL/6) were imaged by MRI every 4 weeks from 8 weeks of age and terminated at 28-30 weeks, or when visual inspection of images indicated unacceptable tumour burden.

**MRI:** MRI was performed on a 7T scanner (Biospec 70/20 Avance III, Bruker Biospin MRI, Ettlingen, Germany) with an 86 mm diameter volume resonator for RF transmission and a phased array mouse heart surface coil for reception. Mice were anesthetised (~2% isoflurane in medical air with 36% $O_2$) for the duration of the MRI scan and positioned on the scanner bed in a prone position. Breathing motion in the pelvic region was reduced by firmly securing the mouse to the scanner bed with adhesive tape across its lower back. The respiration rate was monitored (SA Instruments, USA) and the body temperature was kept at 37 °C by circulating warm water through the bed.

**Low-resolution $T_2$ weighted (LR-T2W):** images were acquired in axial and coronal planes using a RARE spin echo sequence to check correct positioning of the mouse: TE = 36 ms, TR = 5000 ms, RARE factor = 8, averages = 1, slice thickness = 1.0 mm (axial), 0.5 mm (coronal), in-plane resolution 0.15 × 0.15 $mm^2$ (axial), 0.25 × 0.25 $mm^2$ (coronal), acquisition time = 1 min each.

**High-resolution $T_2$ weighted (HR-T2W):** images were acquired in the axial plane using a RARE spin echo sequence, LR-T2W images were used to plan the geometry: TE = 36 ms, TR = 5500 ms, RARE factor = 4, averages = 10, matrix size = 256 × 192, slice thickness = 0.33 mm, in-plane resolution 0.1 × 0.1 $mm^2$, acquisition time = 16 mins.

**DW-MRI:** performed using a Stjeskal-Tanner prepared multi-shot EPI sequence in the axial plane: number of segments = 4, TE = 28.5 ms, TR = 3000 ms, averages = 4, matrix size = 128 × 128, slice thickness = 0.99 mm, in-plane resolution 0.2 × 0.2 $mm^2$, and b-values = 0, 100, 200, 400, 800 $s/mm^2$ along three orthogonal gradient orientations, acquisition time = 10 mins. ADC maps were calculated by voxel-wise fitting of a mono-exponential model to the data using all b-values in MATLAB (MathWorks Inc., USA) and used for regions of interest (ROI) based diffusion analysis.

**Histology & Classification of Mice:** Upon sacrifice, the genitourinary (GU) tract (prostate, seminal vesicles (SV), emptied bladder) was excised, weighed, and fixed in 10% formalin for at least 48 hours. Formalin fixed paraffin embedded samples were sectioned (4 μm slice thickness) and stained with haematoxylin (ChemiTeknik AS, Norway) erythrosine B (Sigma-Aldrich Norway AS) and saffron (ChemiTeknik AS, Norway) using an automatic slide stainer (Sakura Tissue-Tek © Prisma™); HES stained slides were digitised using a Hamamatsu NanoZoomer XR (Hamamatsu, Japan) scanner (40x magnification). Visualisation and annotation of the data was done using Polyzoomer (Institute of Cancer Research, United Kingdom). Two pathologists independently assessed the HES slides, and classified the tumours as either well-differentiated adenocarcinoma (WD), or poorly differentiated carcinoma (PD).

**Registration between MRI and Histology:** HR-T2W and DW-MR images were carefully studied and referenced during paraffin embedding and sectioning to help achieve the optimum sectioning plane. Several histology slides were acquired for each mouse, and HES stained histology sections were correlated with MRI by matching physical landmarks, such as the

urethra, distinctive fluid-filled regions, and general morphology between images.

**MRI assessment of prostate and SV volumes:** HR-T2W images provided good visualisation of mouse prostate (Fig. 1); however, it was difficult to distinguish between prostate tissue and SV at the point of insertion (where SV and prostate lobes meet the urethra). DW-MR images clearly identified the SV, which appeared darker in b800 images than the surrounding prostate. By using b800 images as a reference, whole prostate ROIs (including ventral, lateral, dorsal and anterior lobes) were manually drawn on the HR-T2W axial images using OsiriX (Pixmeo SARL, Switzerland). Seminal vesicle volumes were assessed using manual ROIs drawn on LR-T2W images (OsiriX).

**Diffusion analysis of the whole prostate:** ROIs of the whole prostate (all image slices containing normal prostate and/or PCa) were drawn on b0 images and were used to calculate the median ADC value and ADC histogram of the whole prostate in each animal.

**Diffusion analysis of normal prostate and cancer regions:** Regions of WD cancer, PD cancer, or normal prostate, which were identified by a pathologist on HES histology slides, were correlated to the DW-MR images using physical landmarks. When present, one representative region for each tissue classification was drawn on the b0 image per animal, and the median ADC was calculated for each ROI.

**Prostate cancer screening using DWI:** A screening tool for cancer onset was developed in MATLAB to highlight cancerous prostate regions. The screening tool identified regions in the ADC maps with ADCs below specified threshold values, defined from endpoint DW-MR images.

The first threshold value indicated suspicious regions, defined as the midpoint between normal TRAMP prostate and WD cancer (ADC $\leq 1.2 \times 10^{-3}$ mm$^2$/s), and the second threshold value highlighted regions more likely to be cancer, defined as the midpoint between WD cancer and PD cancer (ADC $\leq 0.78 \times 10^{-3}$ mm$^2$/s). To minimise effect of noise, regions were only highlighted if there were more than 6 adjacent voxels below the threshold value. The algorithm was applied to ADC maps from earlier time points to investigate when the onset of cancer could be determined, and also to investigate when it was possible to differentiate between mice developing aggressive tumours (PD group) from the rest of the TRAMP population (WD group).

**Statistics:** Data are reported as mean ± S.D. and statistical significance between groups was calculated using an unpaired, two-tailed Student's t-test ($p < 0.05$). A Wilcoxon rank sum test was performed for data with too few samples to accurately test for normality.

## Results

**Termination and histological classification:** Cancer onset and growth characteristics varied in the TRAMP mice; following histopathological examination, mice were classified as having WD or PD prostate cancer. The average termination age was 28.3 ± 3.6 weeks (WD group, n = 7) and 20.5 ± 3.5 weeks (PD group, n = 3); C57BL/6 mice were terminated at 30 weeks of age. Fig. 2 shows representative HR-T2W images and corresponding HES histology slices for the three groups.

**Prostate volume:** WD TRAMP prostates grew more rapidly than C57BL/6 controls from 8 weeks of age (Fig. 3a), and were significantly different by 12 weeks ($p = 0.008$). Prostate volumes stabilised in C57BL/6 mice by 24 weeks of age, whereas the TRAMP mouse prostate

volumes continued to increase. Fig. 3b illustrates that three of the TRAMP mice developed fast-growing cancer by 20 weeks (PD group: mice 265, 274, 277). The PD group followed the same growth-curve as the WD group before a large tumour quickly developed; therefore it was not possible to predict which mice would develop aggressive cancer from the total prostate volume. The average prostate volume at termination was $0.13 \pm 0.05$ cm$^3$ (WD, n = 7), $0.42 \pm 0.35$ cm$^3$ (PD, n = 3) and $0.05 \pm 0.01$ cm$^3$ (C57BL/6, n = 6).

**SV volume:** Average SV volume differed considerably between TRAMP and C57BL/6 mice (Fig. 3c). A statistically significant difference in SV volume was measured at 8 weeks ($p = 0.03$, WD and C57BL/6 groups) but became highly significant from 16 weeks ($p = 0.004$). In TRAMP mice both the SV growth rate and the standard deviation increased with age; in contrast, C57BL/6 mice had relatively stable SV volumes. The PD group did not show different trends in SV volume compared with the WD group. SV volume at termination was $1.83 \pm 1.01$ cm$^3$ (WD, n = 7), $0.70 \pm 0.29$ cm$^3$ (PD, n = 3) and $0.36 \pm 0.07$ cm$^3$ (C57BL/6, n = 6).

**SV tumours:** SV tumours developed in 86% (6/7) of WD TRAMP mice, 67% (2/3) of PD TRAMP mice and none of the C57BL/6 mice. Tumours were clearly visible on T2W-MR images at $23 \pm 4$ weeks in WD mice, and at 19 weeks for both of the PD mice. The two mice that did not develop SV tumours were terminated at 21 weeks (WD cancer mouse) and 17 weeks (PD cancer mouse); their relatively young age at death could explain why no tumours were observed.

**GU weight:** Fig. 3d compares the GU weight with the prostate and SV volumes from WD TRAMP, PD TRAMP, and C57BL/6 mice at termination. The GU weight was most strongly correlated with SV volume. GU weight was considerably greater in the WD group than the PD

group, despite the presence of large prostate tumours in the PD group. The average GU weight at termination was 2.08 ± 1.05 g (WD, n = 7), 1.06 ± 0.14 g (PD, n = 3) and 0.53 ± 0.06 g (C57BL/6, n = 6). GU weight normalised to body weight displayed the same trend (Fig. 3d).

**ADCs of the whole prostate:** Median ADC values of TRAMP prostates were significantly lower than C57BL/6 controls from 12 weeks of age ($p = 0.01$ (WD vs. C57BL/6), $p = 0.002$ (WD+PD vs. C57BL/6)) (Fig. 4a). Median prostate ADC values from mice later shown to develop PD cancer (mice 265, 274, 277) decreased with age. WD TRAMPs did not show a significant reduction in median prostate ADC with age. At 16 weeks of age, mouse 274 developed PD cancer, which was clearly identified by a reduction in the median ADC. Median ADCs of mice 277 and 265 were clearly separated from WD mice by 20 weeks. The average median whole prostate ADC of the PD group was very similar at termination ($(0.63 \pm 0.03) \times 10^{-3}$ mm$^2$/s, n = 3), despite differences in onset age and tumour volume. A larger variation in average median whole prostate ADC was observed for both the WD group ($(1.23 \pm 0.16) \times 10^{-3}$ mm$^2$/s, n = 7)), and C57BL/6 mice ($(1.73 \pm 0.20) \times 10^{-3}$ mm$^2$/s, n = 6)), consistent with the heterogeneous nature of prostate tissue observed from histology.

**ADC histograms:** ADC histograms of the entire prostate displayed an obvious shift in the distribution towards lower ADC values as cancer progressed in PD mice (Fig. 4b**)**. Histograms appeared sensitive to distinguishing cancer from prostate tissue, where a bimodal distribution at 20 weeks was visible in the PD cancer mouse. The representative WD cancer ADC histograms showed that the range of ADC values remained unchanged as mice aged, but the skew of the data tended towards lower ADC values for later time points.

**ADCs of normal prostate and cancer regions:** b800 images and ADC maps from the final time point MR scan were used to visualise diffusion characteristics in the prostates; cancerous regions appeared dark on ADC maps and bright on b800 images. In PD TRAMP mice, the median prostate ADC values were fairly homogeneous at the final time point, whereas WD mice were more heterogeneous and displayed regions of low ADC, which were confirmed as cancerous regions from histology. ROIs depicting normal prostate tissue, well-differentiated cancer tissue, and poorly differentiated cancer tissue were drawn on a representative b0 image from each mouse acquired at the final time point MR scan. The mean of the median ADCs were calculated for C57BL/6 prostate ($(1.86 \pm 0.20) \times 10^{-3}$ $mm^2/s$, n = 6), and for the three ROIs in TRAMP prostate: normal prostate ($(1.38 \pm 0.10) \times 10^{-3}$ $mm^2/s$, n = 7), well-differentiated cancer tissue ($(0.93 \pm 0.18) \times 10^{-3}$ $mm^2/s$, n = 7), and poorly differentiated cancer tissue ($(0.63 \pm 0.06) \times 10^{-3}$ $mm^2/s$, n = 3). Fig. 5 indicates that, at termination, the average median ADC of normal TRAMP prostate tissue was significantly lower than for C57BL/6 prostate ($p < 0.001$); ADC of well-differentiated cancer regions was significantly lower than for the normal TRAMP prostate regions ($p < 0.001$), and the average median ADC of poorly differentiated cancer regions was significantly lower than for the well-differentiated cancer regions ($p = 0.02$, Wilcoxon rank sum test). Representative histological images from the different prostate tissues are displayed in Fig. 5, where distinct differences in tissue morphology are evident.

**Prostate cancer screening using DW-MRI:** The screening tool highlighted regions of low ADC in TRAMP prostates, defined according to the median ADC of prostate regions in the paragraph above. The yellow areas in Fig. 6 indicate lower than average median ADC tissue that could be PIN, or onset of well-differentiated cancer, and the red areas illustrate well-differentiated or poorly differentiated cancer. Fig. 6a and 6b depict the development of cancer in representative

PD and WD cancer mice, respectively. The tool identified cancer onset in the PD mouse (Fig. 6a) by 16 weeks, which preceded significant changes in both prostate volume and whole prostate ADC measurements. In the WD mouse, a suspicious transformation of the lateral prostate was identified at 12 weeks of age, which can be seen to develop into cancer by 24 weeks. The screening tool proved useful at highlighting cancerous regions in ADC maps from both PD and WD mice, and the colour map made it easier to track cancer progression.

**Discussion**

The TRAMP model represents a robust experimental platform for the evaluation of novel chemopreventive and therapeutic strategies in PCa (16-18), as it recapitulates the spontaneous development as well as key pathophysiological and morphological characteristics of human PCa progression. In this study we demonstrate the ability of DW-MRI to identify cancer onset and to noninvasively monitor its development to later-stage disease in the TRAMP model. We especially demonstrate the potential of ADC as a biomarker to stratify disease progression from PIN to advanced PCa, and as such its value as a tool for study design and guidance in preclinical trials of novel preventive or therapeutic strategies in TRAMP mice. This will improve the accuracy and relevance of such studies, while reducing the number of animals used.

Our data demonstrate that GU weight is strongly influenced by the SV volume (and therefore SV weight), which increases with age. This trend can partly be attributed to the formation of SV tumours in 80% of TRAMP mice, consistent with the literature (19). As a consequence, variation in the age of the mouse at termination will introduce a high level of inaccuracy in determining prostate tumour burden from GU weight. MRI represents the technique of choice for the evaluation of abdominal malignancies, and anatomical T2W MRI is already used to evaluate

treatment efficacy using the RECIST (Response Evaluation Criteria In Solid Tumors) criteria in TRAMP mice (18). However, T2W MRI is not accurate in distinguishing early stage cancer, or in distinguishing prostate from SV at the point of insertion. Here we demonstrate that the combined use of b800 DW-MR images and T2W images in both axial and coronal planes, accurately discriminate the SV from the prostate, facilitating accurate quantification of prostate volume.

We show that MR-derived prostate volumes increased steadily with age in most TRAMP mice, and were significantly different from C57BL/6 controls after 12 weeks. Three TRAMP mice developed fast-growing cancer originating in the ventral prostate at a young age (PD group). Interestingly, studies have shown that the ventral prostate is least prone to development of PIN lesions, from which prostate cancer is understood to arise (20). The apparent absence of progression from well-differentiated to poorly differentiated cancer in the PD group does not follow the expected trends of cancer progression in the TRAMP mice, and similar observations have been reported in the literature (21,22). The data imply that these mice spontaneously developed aggressive cancer, and could form a sub-type of TRAMP mice.

The success of DW-MRI in the clinical management of PCa can be attributed to a marked contrast in structure between the prostate gland, which is dominated by luminal, fluid filled regions, resulting in characteristically high ADC values ($\sim 1.2 \times 10^{-3}$ mm$^2$/s in our study), and the chaotic and dense cellular structure of the invading malignancies ($<0.7 \times 10^{-3}$ mm$^2$/s for PD cancer). Interestingly, we also show a difference between TRAMP and C57BL/6 (control) whole prostate ADCs, a likely result of increased cellularity in TRAMP prostates, associated with the formation of PIN, which precedes the development of prostate cancer (23). Correlation of ADC maps and b800 images with the histopathologically defined prostate regions demonstrate the

ability of ADC to discriminate between normal TRAMP prostate, well-differentiated adenocarcinoma, and poorly differentiated carcinoma. These ADC values were integrated into an automated threshold tool for monitoring disease onset and progression from ADC maps. This tool identified voxel clusters with low ADC, which were shown to develop into PCa; suspicious regions were highlighted before any changes in the median whole prostate ADC or mean prostate volume were detected in either WD or PD mice cohorts. In particular, for WD mice, the screening tool depicted the formation and progression of cancer, despite that the median ADC for the whole prostate did not significantly change throughout the lifetime of the mice. Detailed information about early events is crucial for design and conduct of clinically relevant studies of chemopreventive agents or novel anticancer drugs in TRAMP mice. The ADC values reported in this study are similar to ADC values reported in the clinic for healthy and diseased prostate (24), supporting the use of the TRAMP model for investigative radiological study, and indicating that DW-MRI is a key modality for use in multiparametric MRI-based active surveillance of patients with low-risk prostate cancer.

**Conclusions**

In this study, we demonstrated that diffusion-weighted MRI and the derived biomarker ADC are robust tools for non-invasively detecting the onset of prostate cancer, and discriminating between well-differentiated adenocarcinoma and poorly differentiated carcinoma in the TRAMP model. Furthermore, detection of voxel clusters with a low median ADC characterised PCa onset prior to morphologic changes. The incorporation of DW-MRI-based PCa stratification and monitoring will increase the accuracy of preclinical trials using TRAMP mice, reduce the number of animals used, and ultimately accelerate the delivery of novel preventive or therapeutic strategies to patients with PCa. Our study suggests that DW-MRI may be useful for longitudinal surveillance

of patients with low-risk prostate cancer, with little cost to patient comfort, and great potential to improve the quality of life by implementation of image-based surveillance as an alternative to radical treatment.

**References:**


1. Torre LA, Bray F, Siegel RL, Ferlay J, Lortet-Tieulent J, Jemal A. Global cancer statistics, 2012. CA: a cancer journal for clinicians 2015;65(2):87-108.
2. Puech P, Rouvière O, Renard-Penna R, et al. Multiparametric MR-targeted Biopsy with Cognitive and Transrectal US–MR Fusion Guidance versus Systematic Biopsy—Prospective Multicenter Study. Radiology 2013;268(2):461-469.
3. Gingrich JR, Greenberg NM. A Transgenic Mouse Prostate Cancer Model. Toxicologic pathology 1996;24(4):502-504.
4. Kaplan-Lefko PJ, Chen TM, Ittmann MM, et al. Pathobiology of autochthonous prostate cancer in a pre-clinical transgenic mouse model. The Prostate 2003;55(3):219-237.
5. Greenberg NM, DeMayo F, Finegold MJ, et al. Prostate cancer in a transgenic mouse. Proceedings of the National Academy of Sciences of the United States of America 1999;92:3439-3443.
6. Gingrich JR, Barrios RJ, Foster BA, Greenberg NM. Pathologic progression of autochthonous prostate cancer in the TRAMP model. Prostate cancer and prostatic diseases 1999;2:70-75.
7. Hurwitz AA, Foster BA, Allison JP, Greenberg NM, Kwon ED. The TRAMP Mouse as a Model for Prostate Cancer. Current Protocols in Immunology 2001;45:1-23.
8. Mazaheri Y, Shukla-Dave A, Muellner A, Hricak H. MR imaging of the prostate in clinical practice. Magma 2008;21(6):379-392.
9. Kurhanewicz J, Vigneron D, Carroll P, Coakley F. Multiparametric magnetic resonance imaging in prostate cancer: present and future. Current opinion in urology 2008;18(1):71-77.
10. Degrassi A, Russo M, Scanziani E, et al. Magnetic resonance imaging and histopathological characterization of prostate tumors in TRAMP mice as model for pre-clinical trials. The Prostate 2007;67(4):396-404.
11. Scheenen TWJ, Rosenkrantz AB, Haider MA, Fütterer JJ. Multiparametric Magnetic Resonance Imaging in Prostate Cancer Management
Current Status and Future Perspectives. Investigative Radiology 2015; (Epub ahead of print).
12. Boesen L, Chabanova E, Logager V, Balslev I, Thomsen HS. Apparent diffusion coefficient ratio correlates significantly with prostate cancer gleason score at final pathology. Journal of magnetic resonance imaging : JMRI 2014.
13. Gatenby RA, Grove O, Gillies RJ. Quantitative Imaging in Cancer Evolution and Ecology. Radiology 2013;269(1):8-15.

14. Gillies RJ, Verduzco D, Gatenby RA. Evolutionary dynamics of carcinogenesis and why targeted therapy does not work. Nature reviews Cancer 2012;12(7):487-493.
15. Zhou M, Hall L, Goldgof D, et al. Radiologically Defined Ecological Dynamics and Clinical Outcomes in Glioblastoma Multiforme: Preliminary Results. Translational Oncology 2014;7(1):5-13.
16. Shukla S, Bhaskaran N, Babcook MA, Fu P, Maclennan GT, Gupta S. Apigenin inhibits prostate cancer progression in TRAMP mice via targeting PI3K/Akt/FoxO pathway. Carcinogenesis 2014;35(2):452-460.
17. Ajibade AA, Kirk JS, Karasik E, et al. Early growth inhibition is followed by increased metastatic disease with vitamin D (calcitriol) treatment in the TRAMP model of prostate cancer. PloS one 2014;9(2):e89555.
18. Arbab AS, Shankar A, Varma NR, et al. MRI to assess chemoprevention in transgenic adenocarcinoma of mouse prostate (TRAMP). BMC medical imaging 2011;11:21.
19. Tani Y, Suttie A, Flake GP, Nyska A, Maronpot RR. Epithelial-stromal tumor of the seminal vesicles in the transgenic adenocarcinoma mouse prostate model. Veterinary pathology 2005;42(3):306-314.
20. Grabowska MM, DeGraff DJ, Yu X, et al. Mouse models of prostate cancer: picking the best model for the question. Cancer metastasis reviews 2014;33(2-3):377-397.
21. Zhang J, Wang L, Zhang Y, et al. Chemopreventive effect of Korean Angelica root extract on TRAMP carcinogenesis and integrative "omic" profiling of affected neuroendocrine carcinomas. Molecular carcinogenesis 2014.
22. Chiaverotti T, Couto SS, Donjacour A, et al. Dissociation of epithelial and neuroendocrine carcinoma lineages in the transgenic adenocarcinoma of mouse prostate model of prostate cancer. The American journal of pathology 2008;172(1):236-246.
23. Jeet V, Russell PJ, Khatri A. Modeling prostate cancer: a perspective on transgenic mouse models. Cancer metastasis reviews 2010;29(1):123-142.
24. Selnæs KM, Heerschap A, Jensen LR, et al. Peripheral Zone Prostate Cancer Localization by Multiparametric Magnetic Resonance at 3 T - Unbiased Cancer Identification by Matching to Histopathology. Investigative Radiology 2012;47(11):624-633.

**Figure Legends**

**Figure 1:** (**a**): Axial HR-T2W images from a 21 week old WD TRAMP mouse; lateral prostate (LP, orange), ventral prostate (VP, green) and dorsal prostate (DP, red) are indicated. The dark green and red lines (labelled 1, 2, respectively) indicate the imaging plane and image slice thickness for the LR-T2W coronal images shown in (**b**). The pairs of orange lines in the coronal images indicate the field of view of the axial image. (**c**) Ventral and dorsal views of the gross anatomy of prostate and SV, note how a lobe of the SV on the right hand side of the ventral

image was twisted downwards, exposing the anterior prostate. Following excision from the mouse (dorsal view), the lobe untwisted, highlighting a difficulty of registering histology and MRI.

**Figure 2**: Registration between HR-T2W MRI and HES histology slices of (**a**) C57BL/6 control mice (30 weeks old) displaying normal mouse prostate anatomy, the ventral and lateral prostate appear brighter in the MRI images, compared with the dorsal prostate (**b**) WD TRAMP (26 weeks old), presenting with tumour arising in the lateral prostate (red arrow) and (**c**) PD TRAMP (24 weeks old), with large PD cancer engulfing the entire prostate. Registration was obtained by matching physical landmarks between MRI and histology, for example the urethra, and liquid region in the WD mouse, indicated with a blue arrow in (**b**).

**Figure 3**: (**a**) Prostate volumes of WD TRAMP (n = 7), and C57BL/6 mice (n = 6), derived from HR-T2W axial images. Owing to WD mice termination: # n = 6, ## n = 5. *p < 0.05, **p < 0.005 (Student's unpaired two-tailed t-test). (**b**) Prostate volumes of individual data points from three TRAMP mice that developed fast growing cancer at a young age; these mice did not fit the trend of the WD group, and form the PD cancer group. (**c**) SV volumes from C57BL/6, WD TRAMP, and PD TRAMP mice. Note that the PD TRAMP mice follow the same trend in SV volume as WD TRAMPs, and that variation in SV volume increases significantly with age. Owing to WD mice termination: # n = 6, ## n = 5. *p < 0.05, **p < 0.005 (Student's unpaired two-tailed t-test) compares WD TRAMP with C57BL/6 data. (**d**) Average prostate volume (P), SV volume, GU weight and normalised GU weight (GU weight/bodyweight, multiplied by 30 for display purposes) for C57BL/6 (n = 6), WD TRAMP (n = 7) and PD TRAMP (n = 3) mice.

**Figure 4**: (**a**) Whole prostate ADCs calculated using all b-values. Owing to WD mice termination: # n = 6, ## n = 5. *p < 0.05, **p < 0.005 (Student's unpaired two-tailed t-test) indicates significant difference between WD TRAMP and C57BL/6 groups. (**b**) Area-normalised ADC histograms from representative PD and WD TRAMP prostates; legend is mouse age (weeks).

**Figure 5**: ADCs from C57BL/6 and TRAMP mice prostate regions at termination. ROIs were drawn on a single, representative slice of the MR image in ventral or lateral prostate. Histology images show examples of the tissue pathology for each of the defined regions (30x magnification). C57BL/6 prostate (grey) was normal ventral or lateral prostate tissue, TRAMP prostate (green) was ventral or lateral prostate tissue that appeared normal on ADC maps and on HR-T2W images, WD (blue) was low-ADC regions corresponding with WD adenocarcinoma on histology, and PD (red) was from mice that developed PD carcinoma. *p < 0.05 (Wilcoxon rank sum test), **p < 0.005 (Student's unpaired two-tailed t-test).

**Figure 6**: Automated cancer screening using ADC maps in PD and WD TRAMP mice. The colour-map highlights regions of ADC falling below a threshold value derived from the ADCs measured from different regions of the TRAMP prostate tissue. Yellow indicates a region of below-normal ADC for ventral/lateral prostate (ADC $\leq 1.2 \times 10^{-3}$ $mm^2/s$) and red indicates cancer (ADC $\leq 0.78 \times 10^{-3}$ $mm^2/s$). (**a**) PD cancer mouse 265: a focal region is evident at 16 weeks old (indicated with *), which was seen to develop into a PD tumour by 20 weeks. (**b**) Representative WD cancer mouse: the lateral prostate in the right side of the image was highlighted yellow from 12 weeks of age (indicated with *), which could be a result of a pre-cancerous transformation of the lateral prostate tissue. This region developed into a cancerous

region by 24 weeks of age, highlighted red. The cancerous region is indicated on the HR-T2W image, ADC map and histology with a red arrow. In all TRAMP mice, the dorsal prostate was highlighted in yellow from a young age, owing to higher cellularity in the morphology of this prostate lobe, rather than from cancer formation.

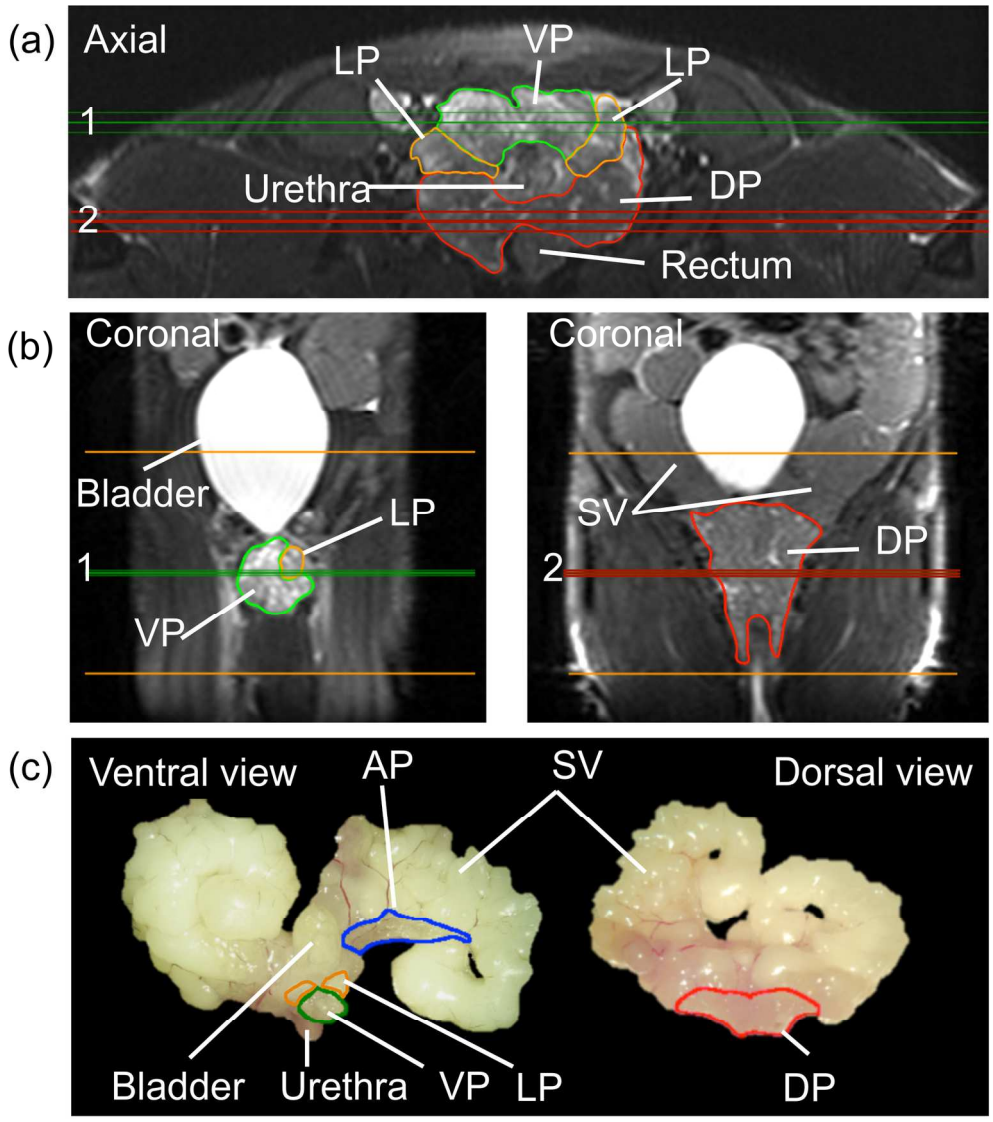


**Figure 1: (a)**: Axial HR-T2W images from a 21 week old WD TRAMP mouse; lateral prostate (LP, orange), ventral prostate (VP, green) and dorsal prostate (DP, red) are indicated. The dark green and red lines (labelled 1, 2, respectively) indicate the imaging plane and image slice thickness for the LR-T2W coronal images shown in **(b)**. The pairs of orange lines in the coronal images indicate the field of view of the axial image. **(c)** Ventral and dorsal views of the gross anatomy of prostate and SV, note how a lobe of the SV on the right hand side of the ventral image was twisted downwards, exposing the anterior prostate. Following excision from the mouse (dorsal view), the lobe untwisted, highlighting a difficulty of registering histology and MRI.
169x188mm (300 x 300 DPI)

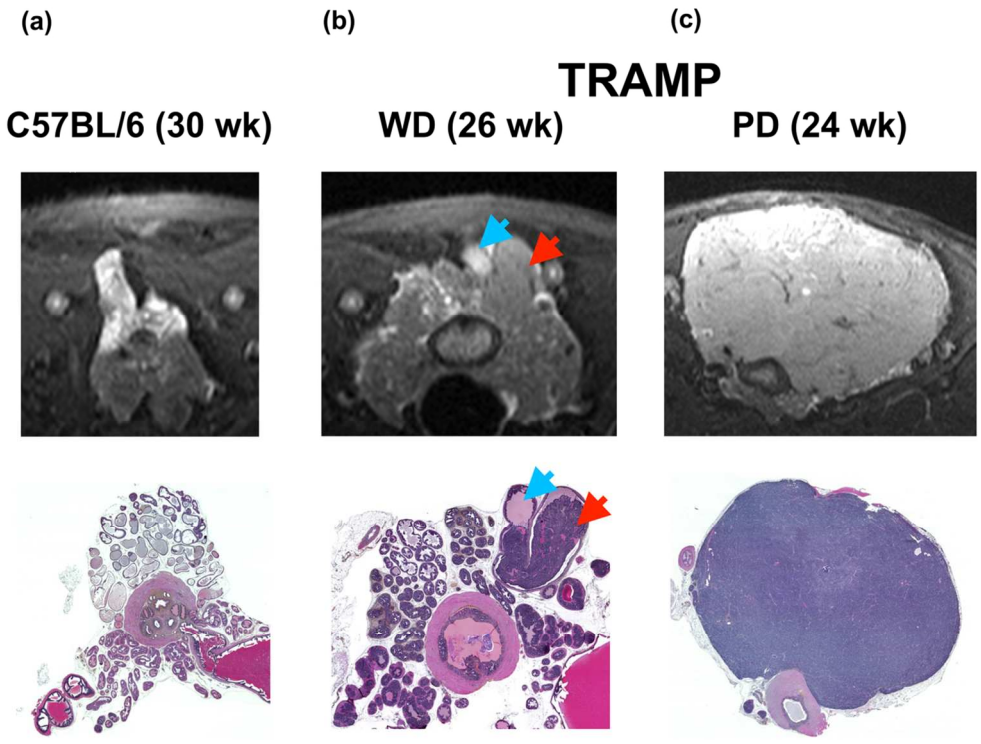


**Figure 2**: Registration between HR-T2W MRI and HES histology slices of **(a)** C57BL/6 control mice (30 weeks old) displaying normal mouse prostate anatomy, the ventral and lateral prostate appear brighter in the MRI images, compared with the dorsal prostate **(b)** WD TRAMP (26 weeks old), presenting with tumour arising in the lateral prostate (red arrow) and **(c)** PD TRAMP (24 weeks old), with large PD cancer engulfing the entire prostate. Registration was obtained by matching physical landmarks between MRI and histology, for example the urethra, and liquid region in the WD mouse, indicated with a blue arrow in **(b)**.
113x83mm (300 x 300 DPI)

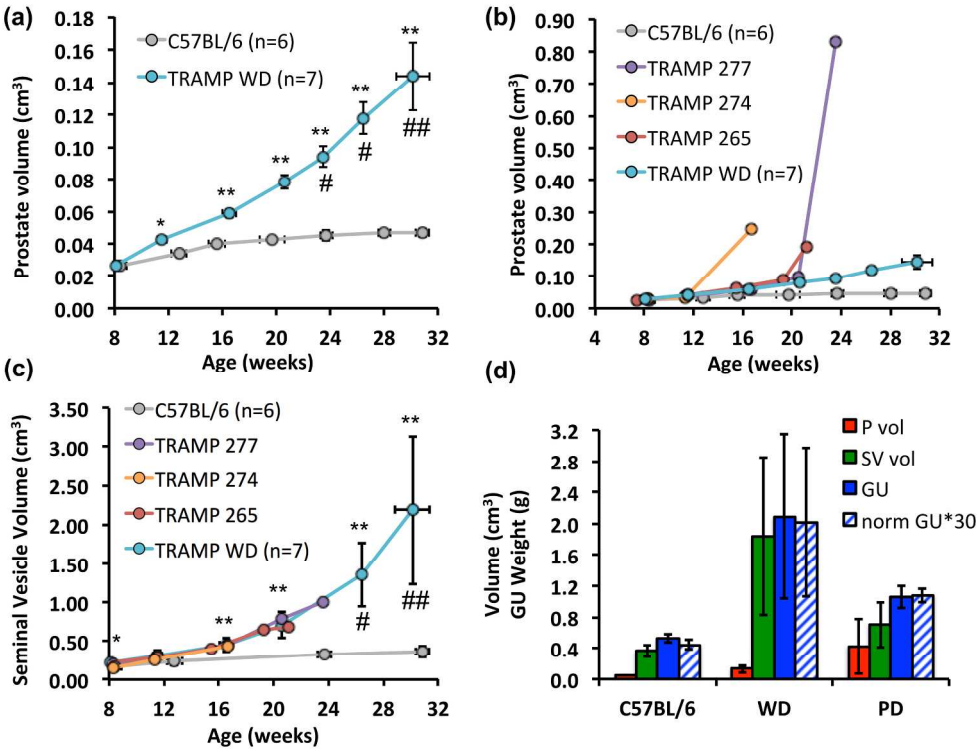


**Figure 3**: **(a)** Prostate volumes of WD TRAMP (n = 7), and C57BL/6 mice (n = 6), derived from HR-T2W axial images. Owing to WD mice termination: # n = 6, ## n = 5. *p < 0.05, **p < 0.005 (Student's unpaired two-tailed t-test). **(b)** Prostate volumes of individual data points from three TRAMP mice that developed fast growing cancer at a young age; these mice did not fit the trend of the WD group, and form the PD cancer group. **(c)** SV volumes from C57BL/6, WD TRAMP, and PD TRAMP mice. Note that the PD TRAMP mice follow the same trend in SV volume as WD TRAMPs, and that variation in SV volume increases significantly with age. Owing to WD mice termination: # n = 6, ## n = 5. *p < 0.05, **p < 0.005 (Student's unpaired two-tailed t-test) compares WD TRAMP with C57BL/6 data. **(d)** Average prostate volume (P), SV volume, GU weight and normalised GU weight (GU weight/bodyweight, multiplied by 30 for display purposes) for C57BL/6 (n = 6), WD TRAMP (n = 7) and PD TRAMP (n = 3) mice.
115x86mm (600 x 600 DPI)

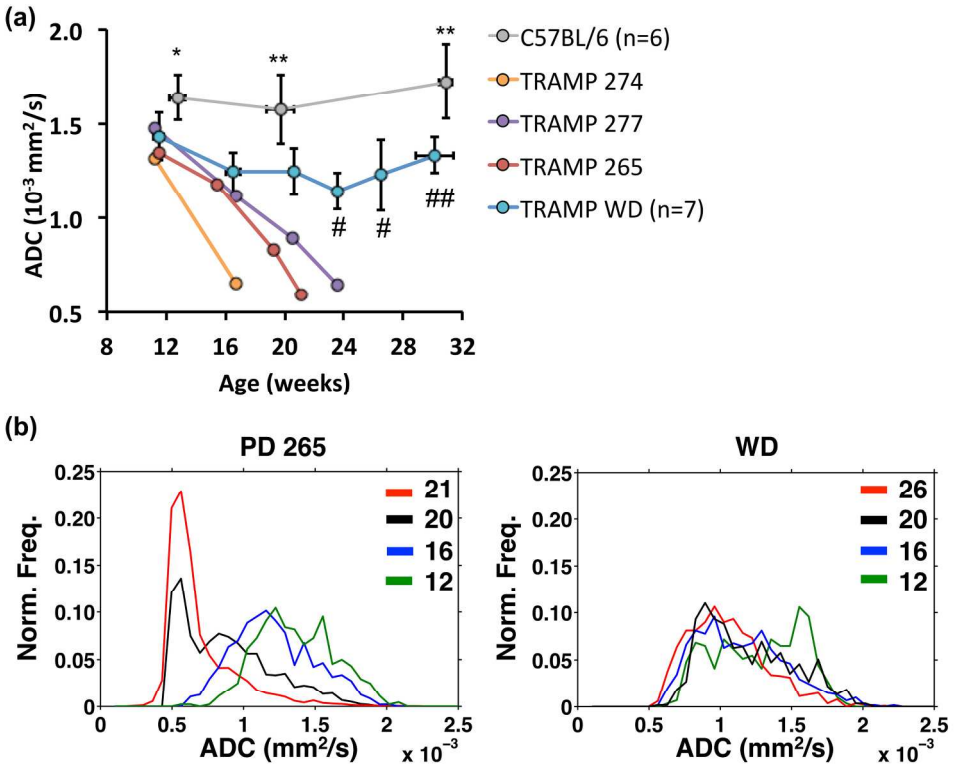


**Figure 4**: **(a)** Whole prostate ADCs calculated using all b-values. Owing to WD mice termination: # n = 6, ## n = 5. *p < 0.05, **p < 0.005 (Student's unpaired two-tailed t-test) indicates significant difference between WD TRAMP and C57BL/6 groups. **(b)** Area-normalised ADC histograms from representative PD and WD TRAMP prostates; legend is mouse age (weeks).
100x80mm (600 x 600 DPI)

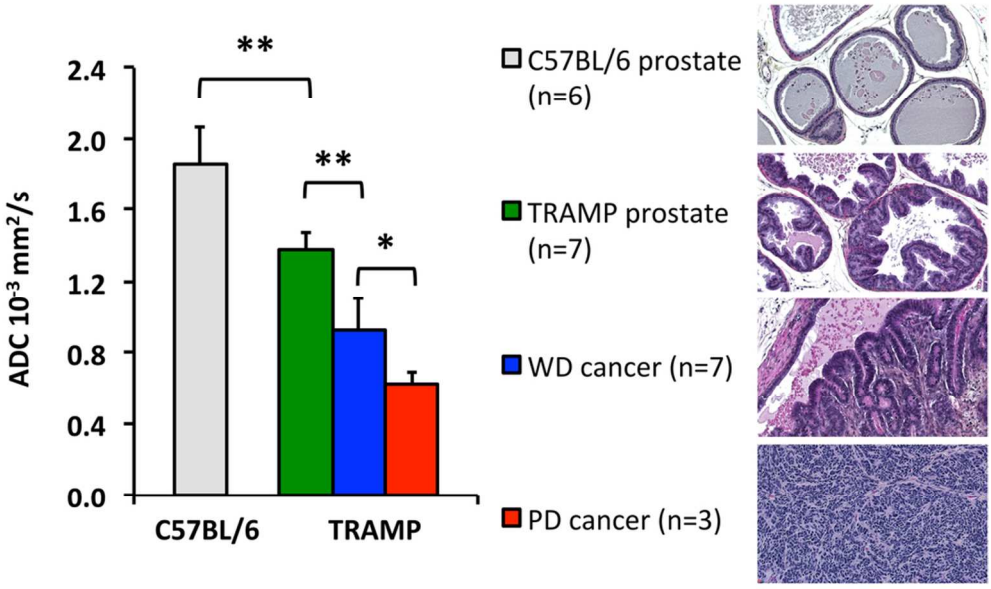


**Figure 5**: ADCs from C57BL/6 and TRAMP mice prostate regions at termination. ROIs were drawn on a single, representative slice of the MR image in ventral or lateral prostate. Histology images show examples of the tissue pathology for each of the defined regions (30x magnification). C57BL/6 prostate (grey) was normal ventral or lateral prostate tissue, TRAMP prostate (green) was ventral or lateral prostate tissue that appeared normal on ADC maps and on HR-T2W images, WD (blue) was low-ADC regions corresponding with WD adenocarcinoma on histology, and PD (red) was from mice that developed PD carcinoma. *p < 0.05 (Wilcoxon rank sum test), **p < 0.005 (Student's unpaired two-tailed t-test).
91x54mm (300 x 300 DPI)

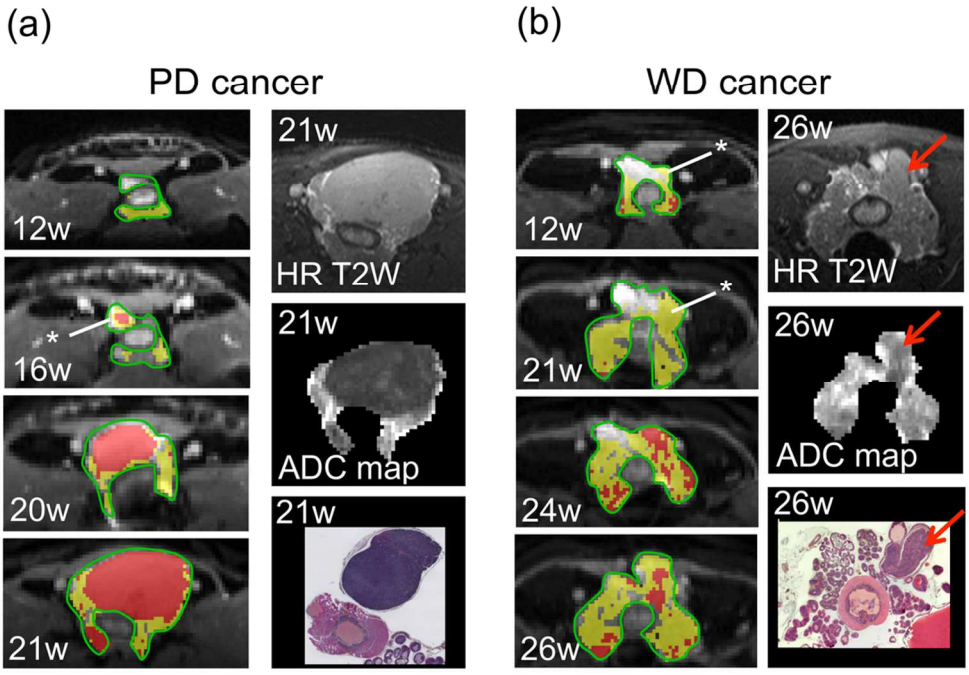


**Figure 6**: Automated cancer screening using ADC maps in PD and WD TRAMP mice. The colour-map highlights regions of ADC falling below a threshold value derived from the ADCs measured from different regions of the TRAMP prostate tissue. Yellow indicates a region of below-normal ADC for ventral/lateral prostate (ADC ≤ $1.2 \times 10^{-3}$ $mm^2/s$) and red indicates cancer (ADC ≤ $0.78 \times 10^{-3}$ $mm^2/s$). **(a)** PD cancer mouse 265: a focal region is evident at 16 weeks old (indicated with *), which was seen to develop into a PD tumour by 20 weeks. **(b)** Representative WD cancer mouse: the lateral prostate in the right side of the image was highlighted yellow from 12 weeks of age (indicated with *), which could be a result of a pre-cancerous transformation of the lateral prostate tissue. This region developed into a cancerous region by 24 weeks of age, highlighted red. The cancerous region is indicated on the HR-T2W image, ADC map and histology with a red arrow. In all TRAMP mice, the dorsal prostate was highlighted in yellow from a young age, owing to higher cellularity in the morphology of this prostate lobe, rather than from cancer formation.
105x72mm (300 x 300 DPI)